NEOPLASMA accepted, ahead of print manuscript
Cite article as https://doi.org/10.4149/neo_2026_251028N451

Running title: V9302 inhibits non-small cell lung cancer

V9302, an inhibitor of glutamine transport, suppresses proliferation and migration, and induces apoptosis in non-small cell lung cancer cells through ROS-mediated mTOR/p70S6K pathway

Shuo Li[1], Xingyu Zhang[1], Teng Chen[1], Xiaofan Cong[1], Wenjing Feng[1], Xiaojin Sun[1,2], Cheng Zha[3], Surong Zhao[1,2,*], Pei Zhang[1,2,*]

[1]School of Pharmacy, Bengbu Medical University, Bengbu, China; [2]Anhui Engineering Technology Research Center of Biochemical Pharmaceuticals, Bengbu, China; [3]Research Center, Bengbu Medical University, Bengbu, China

*Correspondence: 0900032@bbmu.edu.cn; zhangpei880204@126.com

Received October 28, 2025 / Accepted April 9, 2026

This study aimed to investigate the effects and underlying mechanisms of V9302, an inhibitor of glutamine transport, on non-small cell lung cancer (NSCLC) cells. Proliferation was assessed using the cell counting kit-8, colony formation, and EdU assays. Mitochondrial membrane potential was evaluated through JC-1 staining. Cell cycle distribution, apoptosis, and reactive oxygen species (ROS) levels were analyzed by flow cytometry, while migration was assessed using wound healing and Transwell assays. Western blotting was performed to determine protein expression levels. The antitumor efficacy of V9302 *in vivo* was evaluated using a xenograft mouse model with PC-9 cells. The results demonstrated that V9302 inhibited cell proliferation and induced G1-phase arrest in human lung adenocarcinoma PC-9 and A549 cells. Western blotting showed that V9302 significantly inhibited the ASCT2 protein expression in both PC-9 and A549 cells. Additionally, V9302 promoted apoptosis through a mitochondrial-dependent pathway, as evidenced by elevated levels of cleaved PARP, cleaved Caspase 3, cleaved Caspase 9, and Bax. V9302 also suppressed cell migration by downregulating N-cadherin and vimentin expression. Notably, V9302 triggered significant ROS accumulation and inhibited mTOR/p70S6K pathway activation, an effect that was partially restored by N-acetylcysteine, a ROS scavenger. Pretreatment with mTOR activator MHY1485 mitigated the inhibitory effects of V9302 on cell proliferation and migration, as well as its induction of apoptosis. Furthermore, V9302 inhibited tumor growth and induced apoptosis in a xenograft mouse model, without inducing detectable visceral toxicity. In conclusion, these findings demonstrate that V9302 reduces cell proliferation and migration, and causes apoptosis through the ROS-mediated mTOR/p70S6K pathway in NSCLC cells. These findings provide a novel theoretical foundation for advancing both academic and clinical research on NSCLC treatment.

Key words: non-small cell lung cancer; V9302; apoptosis; reactive oxygen species; mTOR/p70S6K pathway

Non-small cell lung cancer (NSCLC) is the predominant subtype of lung cancer, accounting for nearly 85% of all lung cancer cases [1]. As a highly aggressive tumor, NSCLC is often diagnosed at late stages, accompanied by metastases, which limits therapeutic options and leads to poor prognoses [2]. Despite significant advances in cancer research and therapeutic innovations, the 5-year relative survival rate for advanced NSCLC remains limited [3]. Therefore, the identification of novel biomarkers and therapeutic targets, as well as the elucidation of their underlying molecular mechanisms, is vital for improving NSCLC treatment.

Recent studies emphasize the critical role of glutamine in cancer cell metabolism, particularly in energy production, biosynthesis, and the maintenance of cellular homeostasis [4]. Cancer cells exhibit a greater dependence on Gln for survival and proliferation compared to normal cells. To meet their increased demand for Gln, cancer cells upregulate membrane transporters that facilitate Gln import, thereby enhancing the uptake of this critical amino acid [5], these transporters include the alanine-serine-cysteine transporter 2 (ASCT2), SLC6A14 (solute carrier family 6 member 14), and SLC7A6 (solute carrier family 7 member 6) [6]. ASCT2, the primary Gln transporter, is significantly upregulated in various tumor types, and studies have shown that inhibition of ASCT2 activity yields promising antitumor efficacy [7]. V9302, a selective ASCT2 inhibitor, has been demonstrated to reduce cell growth and proliferation, while promoting apoptosis and oxidative accumulation in cancer cells [8]. Nevertheless, the precise function and underlying mechanisms of V9302 in NSCLC remain inadequately understood. Therefore, elucidating the molecular pathways modulated by V9302 is essential for evaluating its therapeutic potential in NSCLC. Studies indicate that physiological levels of reactive oxygen species (ROS) facilitate tumor progression by enhancing proliferation and migration, while supraphysiological ROS accumulation leads to oxidative damage, resulting in growth arrest and apoptosis through the activation of stress response pathways [9, 10]. In addition, ROS activates multiple signaling pathways that regulate cellular stress responses [11]. Notably, the mTOR/p70S6K pathway is frequently hyperactivated in tumors and has emerged as a potential drug target in various malignancies [12-14].

This study aims to characterize the effects of V9302 on proliferation, migration and apoptosis in NSCLC cells, and to investigate the role of ROS and the mTOR/p70S6K pathway in these processes, with the goal of providing new theoretical insights and experimental evidence for the clinical management of NSCLC.

Materials and methods

Cell culture and treatment. PC-9 and A549 cells, human lung adenocarcinoma cell lines obtained from Wuhan Punosai Biotechnology (Wuhan, China), were cultured in RPMI-1640 medium (Gibco, USA) supplemented with 10% fetal bovine serum (FBS, Excell Bio, Shanghai, China) and 1% penicillin-streptomycin (New Cell & Molecular Biotech, Suzhou, China) at 37 °C under standard conditions. Chemical compound included V9302 (#GC34852, Glpbio, Shanghai, China), N-acetylcysteine (NAC) (#HY-B0215, MedChemExpress, Shanghai, China), and MHY1485 (#HY-B0795, MedChemExpress, Shanghai, China).

Cell viability analysis. After seeding in 96-well plates (5,000 cells/well), the cells were treated with V9302. Following a 24 h incubation, the culture medium was carefully removed and replaced with cell counting kit-8 (#K1018, CCK-8, APExBIO, USA) reagent. After incubation at 37 °C for 30 minutes in the dark, optical density (OD) at 450 nm was measured using a microplate reader (Synergy, USA). The half-maximal inhibitory concentration (IC_{50}) was calculated using GraphPad Prism 8 software based on the OD values.

Measurement of Gln and GSH levels. Total Gln and glutathione (GSH) levels were measured using the Gln assay kit (BC5305, Solarbio, Beijing, China) and GSH assay kit (#BC1175, Solarbio, Beijing, China), respectively. After treatment with V9302, PC-9 and A549 cells were lysed and analyzed according to the supplier's protocol. The levels of Gln and GSH were determined by spectrophotometry (Thermo Fisher Scientific, USA) at 450 nm and 412 nm, respectively.

EdU incorporation assay. To detect cell proliferation using an EdU cell proliferation kit (#C0071S, Beyotime, Shanghai, China), cells were plated in confocal dishes (20,000 cells/well) and then treated with the indicated conditions for 24 h. After EdU labelling (10 μM, 2 h, 37 °C), the cells were fixed with 4% paraformaldehyde for 15 min, permeabilized with 0.3% Triton X-100 for 10 min, and then incubated with the click reaction mixture containing Alexa Fluor azide for 30 min at ambient temperature protected from light. Nuclei were stained with 1 μg/ml DAPI for 5 min. Fluorescence images were captured using an Axio Observer.Z1 microscope (Zeiss, Germany), and quantification was performed using Image J software.

Colony formation assay. After seeding PC-9 and A549 cells (500 cells/well in 6-well plates) and allowing for 24 h of attachment, the cells were treated with V9302 for 10 days. Following treatment,

the cells were washed twice with PBS, fixed with 4% formaldehyde for 20 min, stained with 2% crystal violet for 10 min and then photographed. Colony quantification was performed using Image J software across three independent experiments.

Cell cycle analysis. The cell cycle was detected using a cell cycle detection kit (#BB-4104, Bestbio, Shanghai, China). Cells were inoculated in 6-well plates (500,000 cells/well) and cultured with V9302 for 24 h. After trypsinization and PBS washing, the cells were fixed with 70% ethanol at 4 °C overnight. For cell cycle analysis, the fixed cells were co-stained with RNase A and PI for 30 min at 37 °C in the dark [15]. A minimum of 10,000 events/sample were collected using a CytoFLEX flow cytometer (Beckman, USA), and the experiment was independently repeated three times. Data analysis was conducted using FlowJo v10.8.1 software as previously described.

Apoptosis assay. Apoptosis was detected using a cell cycle detection kit (#BB-4101, Bestbio, Shanghai, China). Cells were inoculated in 6-well plates (200,000 cells/well), treated with the indicated conditions for 24 h, and harvested by trypsinization. After a 15 min incubation in the dark with Annexin V-FITC and PI, apoptosis was assessed by analyzing 10,000 events/sample using a CytoFLEX flow cytometer (Beckman, USA) [16]. The experiment was performed in three independent replicates, and data analysis was conducted using FlowJo v10.8.1 software.

Mitochondrial membrane potential (MMP) assay. MMP was assessed using a MMP assay kit (#C2006, Beyotime, Shanghai, China) following the manufacturer's protocol. Cells were seeded in 6-well plates (100,000 cells/well) and treated with V9302 for 24 h. JC-1 staining (10 μM) was carried out at 37 °C for 20 min under dark conditions, followed by fluorescence imaging using an Axio Observer.Z1 fluorescence microscope (Zeiss, Germany). The JC-1 red/green fluorescence intensity ratio, which reflects changes in MMP, was analyzed using Image J software.

Intracellular ROS level measurement. Intracellular ROS levels were detected using a ROS assay kit (#S0033S, Beyotime, Shanghai, China). After a 24 h exposure to the indicated treatment in 6-well plates (200,000 cells/well), cells were processed with DCFH-DA (Beyotime, Shanghai, China,) (37 °C, 30 min), rinsed with serum-free medium to remove excess dye, harvested by trypsinization, and promptly analyzed using a flow cytometer (Beckman, USA). The levels of ROS were quantified using FlowJo v10.8.1 software.

Wound healing assay. Following seeding (500,000 cells/well in 6-well plates) and 24 h of attachment, a uniform scratch was created at 80-90% confluence using a 200 μl pipette tip. After

three PBS washes, the cells were treated with V9302 for 24 h in medium comprising 2% FBS. Wound healing was documented using a microscope (Olympus, Japan) immediately (0 h) and 24 h post-scratch, and the wound closure was quantified using Image J software.

Transwell migration assay. After resuspension in serum-free medium, cells were seeded into the upper chamber (20,000 cells/well), with 10% FBS medium placed in the lower chamber as a chemoattractant. Following a 24 h incubation with the indicated treatment, the membranes were fixed with 4% paraformaldehyde for 15 min, and non-migrated cells were removed by swabbing. Migrated cells were stained with 0.1% crystal violet for 20 min, washed with PBS, and imaged under a microscope (Olympus, Japan) at 200× magnification. Cell numbers were quantified in five random fields per well using Image J software.

Western blotting analysis. After a 24 h incubation with the indicated treatment, cells were lysed using RIPA (#P0013C, Beyotime, Shanghai, China) lysis solution. Protein concentrations were determined using a bicinchoninic acid (BCA) kit (#ST2222-5g, Beyotime, Shanghai, China). Protein (20-30 μg) was separated by SDS-PAGE and electrotransferred to a PVDF membrane. Following blocking with 5% skim milk in TBST, the membrane was incubated sequentially with primary antibodies (4 °C, overnight) and corresponding HRP-labelled secondary antibodies (room temperature, 1 h), followed by visualization using an Enhanced Chemiluminescent (ECL) substrate (#P10100, NCM Biotech, Suzhou, China). Images were captured using a gel imaging system (Sevier, China). Quantitative analysis was performed with Image J software, with GAPDH or β-Tubulin as the loading reference [17]. Antibodies included anti-PARP (#T40050, Abmart, Shanghai, China), anti-ASCT2 (#5345), anti-Bax (#5023), anti-Bcl-2 (#4223), anti-Caspase-3 (#14220), anti-Caspase-9 (#9502), anti-cleaved Caspase-3 (#9661), anti-cleaved Caspase-9 (#7237), anti-β-Tubulin (#2146), anti-mTOR (#2972), anti-phospho-mTOR (#2971), anti-p70S6K (#9202), anti-phospho-p70S6K (#9234) (Cell Signaling Technology), anti-GAPDH (#60004-1-Ig), anti-E-cadherin (#20874-1-AP), anti-N-cadherin (#22018-1-AP), and anti-vimentin (#60330-1-Ig) (Proteintech).

Xenograft mouse model. BALB/c nude mice (SPF grade, female, 4-6 weeks old, weight 18-20 g) were obtained from Hangzhou Ziyuan Laboratory Animal Technology Co. Ltd. The experimental protocol was approved by the Ethics Committee of Bengbu Medical University (Approval No. 2025A819). PC-9 cells (5,000,000 cells suspended in 200 μl Matrigel/PBS) were subcutaneously

implanted into the right flank of the mice. When tumors reached an average volume of approximately 100 mm^3, the animals were randomly assigned to a control group and a V9302 treatment group, with six mice/group. V9302 was administered via intraperitoneal injection at a dose of 50 mg/kg, prepared in a vehicle composed of 5% DMSO, 40% PEG400, and 55% saline. Mice in the control group received an equal volume of vehicle alone. Treatments were performed once daily for 21 consecutive days. Tumor dimensions and body weight were measured every three days by an investigator blinded to group allocation, and tumor volume was calculated using the formula: $V=(\text{length} \times \text{width}^2)/2$. On day 22, mice were humanely euthanized for tumor excision, weighing, and sample collection for subsequent analysis.

Immunohistochemistry (IHC). Tissue sections were exposed to 3% H_2O_2 for endogenous peroxidase activity quenching and subsequently blocked with serum. The sections were then incubated with primary antibodies against Ki67, cleaved Caspase-3 and E-cadherin at 4 °C overnight. After binding with secondary antibodies and 3,3'-Diaminobenzidine (DAB) staining, the sections were imaged using a light microscope (Olympus, Japan).

Terminal deoxynucleotidyl transferase dUTP nick end labeling (TUNEL) assay. Apoptosis in tumor tissues was detected using a TUNEL apoptosis detection kit (#HY-K1091, MedChemExpress, Shanghai, China) according to the manufacturer's protocol. Briefly, paraffin-embedded tissue sections (4 μm) were deparaffinized, rehydrated, and treated with proteinase K. After blocking endogenous peroxidase activity, sections were incubated with biotinylated Nucl. Mix and rTdT at 37 °C for 1 h, followed by streptavidin-HRP. Staining was visualized with DAB, and sections were counterstained with methyl green. Images were captured using an optical microscope [18] (Olympus, Japan).

Hematoxylin-eosin (H&E) staining. After treatment with xylene for transparency, the specimen was paraffin-embedded and sectioned into piece (thickness 4 μm). As described previously [19], the sections were stained with HE and then visualized through a microscope (Olympus, Japan).

Statistical analysis. The quantitative results, presented as mean±SD from triplicate assays, were analyzed using GraphPad Prism 8.0 and SPSS 27 software. Statistical comparisons among groups were performed using one-way ANOVA followed by the LSD test, with $p < 0.05$ considered to indicate a statistically significant difference.

Results

V9302 inhibits the proliferation of NSCLC cells. To assess the cytotoxic effects of V9302 in PC-9 and A549 cells, the cells were exposed to varying concentrations of V9302 for 24 h. The CCK-8 assay demonstrated a concentration-dependent reduction in cell viability in both cell lines (Figure 1B), with IC_{50} values of 13.41±0.45 μM and 20.02±0.73 μM, respectively. To investigate the impact of V9302 on Gln metabolism in A549 and PC-9 cells, we employed Gln assay kit and GSH assay kit to measure intracellular levels of Gln and GSH. The results demonstrated that V9302 significantly reduced the intracellular content of both Gln and GSH (Figures 1C, 1D). Western blotting revealed that V9302 significantly inhibited the expression of ASCT2 protein in both PC-9 and A549 cells (Figures 1E, 1F). Additionally, V9302 treatment decreased the relative proportion of EdU-positive cells and colony formation, as shown by EdU and colony formation assays (Figures 1G, 1H). The cell cycle plays a crucial role in regulating cell proliferation. Flow cytometry findings demonstrated that V9302 triggered G_1-phase arrest in both PC-9 and A549 cells (Figure 1I). These findings suggest that V9302 influences Gln metabolism and inhibits cell proliferation in NSCLC cells.

V9302 induces apoptosis in NSCLC cells. To reveal the effect of V9302 on apoptosis in both cell lines, we performed Annexin V-FITC/PI staining and observed a significant increase in apoptosis rates in the treated cells (Figure 2A). To determine whether V9302-induced apoptosis involved the mitochondrial pathway, we assessed changes in MMP using the JC-1 probe. V9302 treatment significantly reduced the red/green fluorescence intensity ratio, indicating MMP dissipation (Figure 2B). The decrease in the Bcl-2/Bax ratio, along with the cleavage of Caspase-3, Caspase-9, and PARP, plays a critical role in mitochondrial pathway-mediated apoptosis. Western blot analysis demonstrated that V9302 upregulated Bax expression and the cleavage of PARP, Caspase-3, and Caspase-9, while downregulated Bcl-2, PARP, and Caspase-3 expression in the cells, resulting in decreased Bcl-2/Bax ratio (Figure 2C). Collectively, these findings suggest that V9302 induces apoptosis via the mitochondrial pathway in NSCLC cells.

V9302 restrains the migration of NSCLC cells. To test the anti-migratory activities of V9302, we conducted a wound healing assay in both cell lines. V9302 significantly reduced the percentage of wound closure in both cell lines (Figures 3A, 3B). Consistently, Transwell migration assays demonstrated that V9302 treatment markedly inhibited cell migration (Figure 3C, 3D). During

tumor cell migration, E-cadherin expression decreases, disrupting epithelial homeostasis, while N-cadherin and vimentin expression increases, which mediates dynamic adhesion and enhances cell motility. Western blot analysis revealed that V9302 reduced the levels of vimentin and N-cadherin while increasing the expression of E-cadherin in both cell lines (Figure 3E). These findings confirm that V9302 inhibits the migration of NSCLC cells.

V9302 inhibits mTOR/p70S6K pathway through ROS generation in NSCLC cells. Intracellular ROS production is closely linked to Gln metabolism. Flow cytometry analysis showed that V9302 exposure induced marked intracellular ROS accumulation in both PC-9 and A549 cells. (Figure 4A). Furthermore, previous studies have demonstrated that ROS modulates multiple signaling cascades, with elevated ROS levels inhibiting the function of the mTOR/p70S6K pathway. Western blot analysis confirmed that V9302 significantly decreased the levels of p-mTOR and p-p70S6K, while exerting no marked effect on the total levels of mTOR and p70S6K in the cells (Figure 4B). Pre-treatment with the ROS scavenger NAC, partially reversed V9302-induced suppression of p-mTOR and p-p70S6K in both cell lines (Figure 4C, 4D). These findings suggest that V9302 inhibits the activation of the mTOR/p70S6K pathway through a ROS-dependent mechanism.

V9302 modulates proliferation, migration and apoptosis through mTOR/p70S6K pathway in NSCLC cells. To further elucidate the function of mTOR/p70S6K pathway in V9302-mediated suppression of NSCLC cell proliferation, we treated A549 and PC-9 cells with the mTOR activator MHY1485. EdU incorporation and CCK-8 assays revealed that MHY1485 partially restored V9302-induced inhibition of proliferation in both cell lines (Figures 5A-5C). Meanwhile, MHY1485 attenuated V9302-induced apoptosis (Figure 5D), as evidenced by decreased cleavage of PARP, Caspase-3, and Caspase-9 (Figure 5E). We then examined whether MHY1485 could reverse V9302-mediated inhibition of migration. Transwell assays showed that MHY1485 significantly alleviated V9302-induced suppression of migration (Figure 6A). Furthermore, MHY1485 partially restored E-cadherin level and increased the expression of vimentin and N-cadherin levels (Figure 6B). Collectively, these results demonstrate that V9302 modulates cell migration, proliferation, and apoptosis through the mTOR/p70S6K signaling pathway in NSCLC cells.

V9302 represses the growth of xenografted NSCLC cells *in vivo*. To assess the antitumor activity of V9302 *in vivo*, a xenograft model using PC-9 cells was established in nude mice. V9302 treatment significantly inhibited tumor growth, with both tumor size and weight being dramatically

reduced compared to the control group (Figures 7A, 7C, 7D), while no significant differences in body weight were observed between the V9302 and control groups (Figure 7B). To assess potential hepatotoxicity and nephrotoxicity, we measured corresponding serum indicators such as alanine aminotransferase (ALT), aspartate aminotransferase (AST), creatinine (CRE), blood urea nitrogen (BUN) by ELISA. No significant differences in these indicators were observed between the V9302 and control groups (Figure 7E). Histopathological analysis of important organs (liver, spleen, kidney, lung, and heart) using HE staining showed no significant toxicity in V9302-treated mice compared to the control group (Figure 7F). TUNEL staining revealed a significantly higher apoptosis index in the V9302-treated group compared to the control group (Figures 7G, 7H). Furthermore, IHC analysis demonstrated a marked reduction in Ki67 expression, along with significant upregulation of E-cadherin and cleaved Caspase-3 levels (Figures 7I, 7J). Taken together, these findings suggest that V9302 exerts anti-tumor effects in NSCLC *in vivo*.

Discussion

Recent studies have highlighted the reprogramming of Gln transporters as a critical mechanism in cancer therapy, given that Gln uptake and utilization are essential for the survival and proliferation of cancer cells [7]. Among these transporters, ASCT2 plays a central role in regulating intracellular Gln levels [7]. ASCT2 is significantly upregulated in multiple cancers, including colorectum, prostate, and breast cancers, and its expression is strongly correlated with cancer cell proliferation, invasion, and metastasis [20-23]. Therefore, inhibition of ASCT2 has demonstrated strong anti-tumor effects. ASCT2 inhibitors, such as benzelserine and L-γ-glutamyl-p-nitroanilide, have been developed and are currently undergoing clinical evaluation [24, 25]. However, subsequent studies have demonstrated that these compounds are not suitable for specifically targeting Gln addiction via ASCT2 in tumor cells, due to their low binding affinity, lack of specificity, and the need for high effective doses [21, 25-27]. Notably, a novel ASCT2 inhibitor, V9302, has shown significant anti-tumor activity across a range of cancers, including glioma and renal cell carcinoma, by effectively inhibiting tumor growth [28-30].

V9302 is the first specific and effective small-molecule inhibitor of ASCT2, which inhibits tumor growth by suppressing ASCT2-mediated Gln uptake, thereby affecting intracellular Gln metabolism, inhibiting cell proliferation, and inducing apoptosis [8]. Our findings demonstrate that V9302 exerts

potent anti-tumor effects in NSCLC through dual mechanisms: metabolic disruption and proliferation suppression. By competitively inhibiting Gln uptake, V9302 not only depletes intracellular GSH pools and disrupts energy metabolism but also significantly reduces tumor growth and Ki67 expression *in vivo*. These findings underscore the dependence of NSCLC on Gln for both antioxidant defense (GSH synthesis) and bioenergetics, suggesting that inhibition of Gln transporters may overcome the limitations of targeting downstream enzymes alone.

Furthermore, studies have demonstrated that V9302 disrupts the biosynthesis of key proteins during the G_1/S transition, leading to G_1-phase arrest and subsequent suppression of cell proliferation [31, 32]. This form of sustained growth arrest is a hallmark of cellular senescence, a state that acts as a critical barrier to tumor initiation by engaging tumor suppressor pathways such as p53/p21 [33]. In this study, cell cycle analysis revealed a significant accumulation in the G_1-phase, indicating that the G_1-phase arrest induced by V9302 resulted in reduced proliferation of NSCLC cells. This finding provides a mechanistic explanation for the compound's anti-proliferative effects, as Gln depletion likely disrupts the biosynthesis of key proteins required for the G_1/S transition. Additionally, previous studies have demonstrated that V9302 caused PARP cleavage in breast cancer cells, promoting apoptosis [34], further suggesting its pro-apoptotic potential. Apoptosis is predominantly mediated through the mitochondrial pathway, which is regulated by mitochondrial membrane integrity and the ratio of Bcl-2 family proteins. Mitochondrial damage has emerged as a crucial mechanism for tumor suppression, as it disrupts cellular homeostasis and triggers cell death [35]. The increased Bax/Bcl-2 ratio destabilizes the mitochondrial outer membrane, leading to the breakdown of MMP and cytochrome C efflux, which subsequently triggers the activation of Caspase-9 and Caspase-3, culminating in PARP cleavage, a hallmark of apoptotic cell death [36-38]. In this study, V9302 upregulated Bax expression while downregulating Bcl-2, resulting in a reduction in MMP, followed by the cleavage of PARP, Caspase-3, and Caspase-9. Furthermore, V9302 increased cleaved Caspase-3 levels and enhanced apoptosis index of tissue cells *in vivo*. These findings not only confirm V9302's pro-apoptotic effects across various cancer types but also mechanistically link its metabolic inhibition (Gln uptake blockade) to the activation of intrinsic apoptosis, suggesting a coordinated dual action that amplifies its therapeutic potential against NSCLC.

Beyond its antiproliferative effects, V9302 has been shown to modulate cancer cell migration [39].

Tumor cell migration is a complex process facilitated by dynamic remodeling of the cytoskeleton, extracellular matrix degradation, changes in adhesion, and epithelial-mesenchymal transition, ultimately leading to the acquisition of motility, invasion and metastasis [40]. These processes are characterized by distinct molecular changes, including reduced E-cadherin expression, which disrupts cell adhesion, the disassembly of intercellular connections, and the initial dissociation of epithelial cells. Meanwhile, the levels of vimentin and N-cadherin increases, enhancing matrix degradation and promoting metastatic potential [41]. In this study, V9302 inhibited cell migration by upregulating E-cadherin expression and downregulating vimentin and N-cadherin levels in both cell lines.

As is well known, the oxidative system and its gene regulatory factors play crucial roles in various types of tumors. Disruption or loss of their normal functions can lead to alterations in cell metabolism, proliferation, and apoptosis [42]. ROS production is triggered by various cellular stress conditions, such as impaired mitochondrial function and DNA damage [43]. In the present study, V9302-mediated inhibition of Gln transport significantly impaired Gln metabolism and depleted intracellular GSH levels. The depletion of GSH compromises cellular antioxidant capacity, resulting in ROS accumulation, oxidative stress, and consequent redox imbalance within the cells [39]. Therefore, we performed further validation and found that V9302 significantly increased the intracellular ROS levels in PC-9 and A549 cells, suggesting that the anti-tumor effect of V9302 on NSCLC may be associated with the disruption of intracellular redox homeostasis through ROS accumulation. ROS are known to regulate cell death by modulating multiple signaling pathways, such as the mTOR pathway. Within the complex landscape of redox biology, ROS regulate mTOR signaling through multiple upstream mechanisms. Specifically, H_2O_2 can trigger AMPK activation to modulate mTORC1 via regulatory-associated protein of mTOR (Raptor) phosphorylation, although this effect exhibits notable cell-type specificity. Additionally, oxidative stress may directly engage the PI3K/Akt pathway to stimulate mTOR activity. A critical node for redox input is the tuberous sclerosis complex (TSC); ROS can activate TSC2 to suppress mTORC1 and, in response to oxidative stress, dynamically recruit the TSC complex to peroxisomes to induce autophagy. At the transcriptional level, the master redox regulator NRF2 directly modulates mTOR expression [44-46]. As a critical regulator of cellular homeostasis, mTOR, a serine/threonine protein kinase, governs protein synthesis, cell growth, proliferation, and apoptotic death [47]. Furthermore,

p70S6K, a key downstream factor in the mTOR pathway, plays a major role in regulating translation [48]. The mTOR-mediated phosphorylation of p70S6K to form p-p70S6K promotes tumor progression by enhancing proliferation, invasion, metastasis, and altered metabolism [49]. Extensive research has demonstrated that mTOR/p70S6K is hyperactivated in various malignancies, including breast, prostate, and cervix cancers, positioning it as a promising therapeutic target [48, 50, 51]. Our results demonstrate that V9302 substantially downregulate the expression of p-p70S6K and p-mTOR in both cell lines, indicating the potential of V9302 in the treatment of NSCLC. To investigate whether ROS mediated the effect of V9302 on mTOR/p70S6K, we found that NAC pretreatment abrogated V9302-induced suppression of mTOR/p70S6K signaling. These findings demonstrate that V9302 inhibits mTOR/p70S6K signaling through ROS-dependent mechanisms, as evidenced by the NAC-mediated reversal of this effect. This provides mechanistic insight into V9302's antitumor activity, highlighting oxidative stress as a critical mediator of its metabolic interference in NSCLC.

As a key regulator of tumor progression, mTOR/p70S6K pathway modulates cell proliferation, metastasis, and apoptosis [52, 53]. This pathway promotes cell cycle progression and inhibits mitochondrial-dependent apoptosis by regulating the levels of cyclin-dependent kinases, the Bcl-2/Bax ratio, and other proteins through phosphorylation [54, 55]. Furthermore, the mTOR/p70S6K pathway contributes to tumor metastasis by regulating epithelial-mesenchymal transition [56]. Notably, MHY1485, an agonist of mTOR activation, partially rescues drug-induced inhibition of tumor cells [57]. Our findings demonstrate that V9302 effectively targets this critical pathway, with MHY1485-mediated mTOR activation significantly attenuating V9302's anti-tumor effects on cell migration, proliferation, and apoptosis. This pharmacological rescue experiment provides compelling evidence that mTOR/p70S6K inhibition represents a primary mechanism underlying V9302's therapeutic activity. These results position mTOR/p70S6K inhibition as a promising strategy for concurrently targeting multiple hallmarks of cancer, warranting further investigation into its clinical applications, particularly in combination with existing targeted therapies.

In summary, V9302 inhibits proliferation and migration; while enhancing apoptosis in NSCLC cells, an effect associated with the inhibition of mTOR and p70S6K phosphorylation through ROS accumulation. (Figure 8). This study provides an experimental foundation and novel insights into

the potential use of V9302 for the treatment of NSCLC.

Acknowledgements: We would like to thank Research Center, Bengbu Medical University for providing valuable instruments.

This work was supported by the Natural Science Research Project of Anhui Educational Committee (KJ2021A0736), Natural Science of Bengbu Medical University (2024byzd031, 2023byzd044), and College Student Innovation and Entrepreneurship Training of Anhui Province (S202410367059).

References

[1] MOLINA JR, YANG P, CASSIVI SD, SCHILD SE, ADJEI AA. Non–small cell lung cancer: epidemiology, risk factors, treatment, and survivorship 2009. J Thorac Oncol 2014;9(8):1081-1090. https://doi.org/10.1097/JTO.0000000000000213

[2] YIN X, CUI Y, KIM RS, STILES WR, PARK SH et al. Image-guided drug delivery of nanotheranostics for targeted lung cancer therapy. Theranostics 2022; 12: 4147-4162. https://doi.org/10.7150/thno.72803

[3] HE Y, JIANG X, DUAN L, XIONG Q, YUAN Y et al. LncRNA PKMYT1AR promotes cancer stem cell maintenance in non-small cell lung cancer via activating wnt signaling pathway. Mol Cancer 2021; 20: 156. https://doi.org/10.1186/s12943-021-01469-6

[4] ALTMAN BJ, STINE ZE, DANG CV. From Krebs to clinic: glutamine metabolism to cancer therapy. Nat Rev Cancer 2016; 16: 619-634. https://doi.org/10.1038/nrc.2016.71

[5] BHUTIA YD, BABU E, RAMACHANDRAN S, GANAPATHY V. Amino Acid Transporters in Cancer and Their Relevance to "Glutamine Addiction": Novel Targets for the Design of a New Class of Anticancer Drugs. Cancer Research 2015; 75: 1782-1788. https://doi.org/10.1158/0008-5472.CAN-14-3745

[6] TAMBAY V, RAYMOND VA, VOISIN L, MELOCHE S, BILODEAU M. Reprogramming of glutamine amino acid transporters expression and prognostic significance in hepatocellular carcinoma. Int J Mol Sci 2024; 25: 7558-7577. https://doi.org/10.3390/ijms25147558

[7] TEIXEIRA E, SILVA C, MARTEL F. The role of the glutamine transporter ASCT2 in antineoplastic therapy. Cancer Chemother Pharmacol 2021; 87: 447-464. https://doi.org/10.1007/s00280-020-04218-6

[8] SCHULTE ML, FU A, ZHAO P, LI J, GENG L et al. Pharmacological blockade of ASCT2-dependent glutamine transport leads to antitumor efficacy in preclinical models. Nat Med 2018; 24: 194-202. https://doi.org/10.1038/nm.4464

[9] CUI Q, WANG JQ, ASSARAF YG, REN L, GUPTA P et al. Modulating ROS to overcome multidrug resistance in cancer. Drug Resist Updat 2018; 41: 1-25. https://doi.org/10.1016/j.drup.2018.11.001

[10] SRINIVAS US, TAN BWQ, VELLAYAPPAN BA, JEYASEKHARAN AD. ROS and the DNA damage response in cancer. Redox Biol 2019; 25: 101084. https://doi.org/10.1016/j.redox.2018.101084

[11] MAKHOV P, GOLOVINE K, TEPER E, KUTIKOV A, MEHRAZIN R et al. Piperlongumine promotes autophagy via inhibition of akt/mTOR signalling and mediates cancer cell death. Br J Cancer 2014; 110: 899-907. https://doi.org/10.1038/bjc.2013.810

[12] ZHANG X, LIU H, WANG H, ZHAO R, LU Q et al. B3galt5 deficiency attenuates hepatocellular carcinoma by suppressing mTOR/p70s6k-mediated glycolysis. Cell Mol Life Sci 2023; 80: 8. https://doi.org/10.1007/s00018-022-04601-x

[13] LIU R, ZHANG B, ZOU S, CUI L, LIN L et al. Ginsenoside Rg1 induces autophagy in colorectal cancer through inhibition of the akt/mTOR/p70S6K pathway. J Microbiol Biotechnol 2024; 34: 774-782. https://doi.org/10.4014/jmb.2310.10043

[14] YANG T, XIAO Y, LIU S, LUO F, TANG D et al. Isorhamnetin induces cell cycle arrest and apoptosis by triggering DNA damage and regulating the AMPK/mTOR/p70S6K signaling pathway in doxorubicin-resistant breast cancer. Phytomedicine 2023; 114: 154780. https://doi.org/10.1016/j.phymed.2023.154780

[15] VULETIC A, KONJEVIC G, MILANOVIC D, RUZDIJIC S, JURISIC V. Antiproliferative effect of 13-cis-retinoic acid is associated with granulocyte differentiation and decrease in cyclin B1 and bcl-2 protein levels in G0/G1 arrested HL-60 cells. Pathol Oncol Res 2010; 16: 393-401. https://doi.org/10.1007/s12253-009-9241-2

[16] RADENKOVIĆ N, MILUTINOVIĆ M, NIKODIJEVIĆ D, JOVANKIĆ J, JURIŠIĆ V. Sample preparation of adherent cell lines for flow cytometry: protocol optimization-our experience with SW-480 colorectal cancer cell line. Indian J Clin Biochem 2025; 40: 74-79. https://doi.org/10.1007/s12291-023-01161-0

[17] JURISIC V, SRDIC-RAJIC T, KONJEVIC G, BOGDANOVIC G, COLIC M. TNF-α induced apoptosis is accompanied with rapid CD30 and slower CD45 shedding from K-562 cells. J Membr Biol 2011; 239: 115-122. https://doi.org/10.1007/s00232-010-9309-7

[18] MOON JM, LEE SW, JANG YS, LEE SA, JUNG SH, KIM SK, et al. Gossypin induces apoptosis and autophagy via the MAPK/JNK pathway in HT-29 human colorectal cancer cells. Int J Mol Med 2025; 56: 1-14. https://doi.org/10.3892/ijmm.2025.5548

[19] MA Y, QI Y, ZHOU Z, YAN Y, CHANG J et al. Shenqi fuzheng injection modulates tumor fatty acid metabolism to downregulate MDSCs infiltration, enhancing PD-L1 antibody inhibition of intracranial growth in melanoma. Phytomedicine 2024; 122: 155171. https://doi.org/10.1016/j.phymed.2023.155171

[20] LIU T, WU X, LI Y, LU W, ZHENG F et al. RBFOX3 Regulates the Chemosensitivity of Cancer Cells to 5-Fluorouracil via the PI3K/AKT, EMT and Cytochrome-C/Caspase Pathways. Cell Physiol Biochem 2018; 46: 1365-1380. https://doi.org/10.1159/000489153

[21] VAN GELDERMALSEN M, WANG Q, NAGARAJAH R, MARSHALL AD, THOENG A et al. ASCT2/SLC1A5 controls glutamine uptake and tumour growth in triple-negative basal-like breast cancer. Oncogene 2016; 35: 3201-3208. https://doi.org/10.1038/onc.2015.381

[22] YAO L, WU J, WANG X, WANG N. LINC01134 directly binds and regulates SLC1A5 stability to promotes colorectal cancer progression. J Cancer 2024; 15: 6135-6147. https://doi.org/10.7150/jca.100147

[23] WANG Q, HARDIE R, HOY AJ, VAN GELDERMALSEN M, GAO D et al. Targeting ASCT2 - mediated glutamine uptake blocks prostate cancer growth and tumour development. J Pathol 2015; 236: 278-289. https://doi.org/10.1002/path.4518

[24] SCHULTE ML, KHODADADI AB, CUTHBERTSON ML, SMITH JA, MANNING HC. 2-amino-4-bis(aryloxybenzyl)aminobutanoic acids: a novel scaffold for inhibition of ASCT2-mediated glutamine transport. Bioorg Med Chem Lett 2016; 26: 1044-1047. https://doi.org/10.1016/j.bmcl.2015.12.031

[25] WANG Q, BEAUMONT KA, OTTE NJ, FONT J, BAILEY CG et al. Targeting glutamine transport to suppress melanoma cell growth. Int J Cancer 2014; 135: 1060-1071. https://doi.org/10.1002/ijc.28749

[26] BRÖER A, RAHIMI F, BRÖER S. Deletion of amino acid transporter ASCT2 (SLC1A5) reveals an essential role for transporters SNAT1 (SLC38A1) and SNAT2 (SLC38A2) to sustain glutaminolysis in cancer cells. J Biol Chem 2016; 291: 13194-13205. https://doi.org/10.1074/jbc.M115.700534

[27] GREWER C, GRABSCH E. New inhibitors for the neutral amino acid transporter ASCT2 reveal its na+ - dependent anion leak. J Physiol 2004; 557: 747-759. https://doi.org/10.1113/jphysiol.2004.062521

[28] SZEMERÉDI N, SCHELZ Z, HORVATH DA, RÁCZ B, SZATMÁRI AG et al. Impact of V9302, a Competitive Antagonist of Transmembrane Glutamine Flux on Reversal of Resistance in Breast Cancer Cell Lines. Pharmaceutics 2024; 16: 877. https://doi.org/10.3390/pharmaceutics16070877

[29] HAN L, ZHOU J, LI L, WU X, SHI Y et al. SLC1A5 enhances malignant phenotypes through modulating ferroptosis status and immune microenvironment in glioma. Cell Death Dis 2022; 13: 1071. https://doi.org/10.1038/s41419-022-05526-w

[30] KAWAKAMI I, YOSHINO H, FUKUMOTO W, TAMAI M, OKAMURA S et al. Targeting of the glutamine transporter SLC1A5 induces cellular senescence in clear cell renal cell carcinoma. Biochem Biophys Res Commun 2022; 611: 99-106. https://doi.org/10.1016/j.bbrc.2022.04.068

[31] LI S, ZHOU Q, LIU W, FU Z, ZHAO H et al. Targeting SLC1A5 blocks cell proliferation through inhibition of mTORC1 in arsenite-treated human uroepithelial cells. Toxicol Lett 2021; 345: 1-11. https://doi.org/10.1016/j.toxlet.2021.03.007

[32] HARADA E, YOSHIDA S, IMAIZUMI Y, KAWAMURA A, OHTSUKA T et al. Dual-specificity tyrosine-regulated kinase 2 exerts anti-tumor effects by induction of G1 arrest in lung adenocarcinoma. Biochim Biophys Acta Gen Subj 2024; 1868: 130600. https://doi.org/10.1016/j.bbagen.2024.130600

[33] CHEN Q, LIU J, WU J, XIANG X, ZHOU X et al. Cellular senescence in cancer: Friend or fraud? Drug Resist Updat 2026; 86:101363. https://doi.org/10.1016/j.drup.2026.101363

[34] LI Q, ZHONG X, YAO W, YU J, WANG C et al. Inhibitor of glutamine metabolism V9302 promotes ROS-induced autophagic degradation of B7H3 to enhance antitumor immunity. J Biol Chem 2022; 298:101753. https://doi.org/10.1016/j.jbc.2022.101753

[35] PAN Y, WEI J, QIN D, ZHOU X, GAO F et al. Prosapogenin CP4 exacerbates mitophagy to induce apoptosis via AMPK-mTOR and PINK1/parkin pathways in A549 cells. Phytomedicine 2025; 148: 157333. https://doi.org/10.1016/j.phymed.2025.157333

[36] ZHAO Y, JING Z, LV J, ZHANG Z, LIN J et al. Berberine activates caspase-9/cytochrome c-mediated apoptosis to suppress triple-negative breast cancer cells in vitro and in vivo. Biomed Pharmacother 2017; 95: 18-24. https://doi.org/10.1016/j.biopha.2017.08.045

[37] GAIDT MM, HORNUNG V. Pore formation by GSDMD is the effector mechanism of pyroptosis. EMBO J 2016; 35: 2167-2169. https://doi.org/10.15252/embj.201695415

[38] GAO C, ZHOU Y, LI H, CONG X, JIANG Z et al. Antitumor effects of baicalin on ovarian cancer cells through induction of cell apoptosis and inhibition of cell migration in vitro. Mol Med Rep 2017; 16: 8729-8734. https://doi.org/10.3892/mmr.2017.7757

[39] JAGGUPILLI A, LY S, NGUYEN K, ANAND V, YUAN B et al. Metabolic stress induces GD2+ cancer stem cell-like phenotype in triple-negative breast cancer. Br J Cancer 2022; 126: 615-627. https://doi.org/10.1038/s41416-021-01636-y

[40] YILMAZ M, CHRISTOFORI G. EMT, the cytoskeleton, and cancer cell invasion. Cancer Metastasis Rev 2009; 28: 15-33. https://doi.org/10.1007/s10555-008-9169-0

[41] LI X, ZENG X. Shikonin suppresses progression and epithelial–mesenchymal transition in hepatocellular carcinoma (HCC) cells by modulating miR- 106b/SMAD7/TGF- β signaling pathway. Cell Biol Int 2020; 44: 467-476. https://doi.org/10.1002/cbin.11247

[42] TODOSIJEVIĆ JOVANOVIĆ J, GAŠIĆ V, GRUBIŠA I, ZUKIĆ B, GRZYBOWSKA-SZATKOWSKA L et al. Significance of GSTM1 and GSTT1 gene deletions in glioma patients in polish population: pilot study. Clin Med Insights Oncol 2025; 19: 11795549251330712. https://doi.org/10.1177/11795549251330712

[43] SCHERZ-SHOUVAL R, ELAZAR Z. Regulation of autophagy by ROS: physiology and pathology. Trends Biochem Sci 2011; 36: 30-38. https://doi.org/10.1016/j.tibs.2010.07.007

[44] TENG JF, MEI QB, ZHOU XG, TANG Y, XIONG R et al. Polyphyllin VI induces caspase-1-mediated pyroptosis via the induction of ROS/NF-κB/NLRP3/GSDMD signal axis in non-small cell lung cancer. Cancers (Basel) 2020; 12: 193. https://doi.org/10.3390/cancers12010193

[45] GLORIEUX C, ENRÍQUEZ C, BUC CALDERON P. The complex interplay between redox dysregulation and mTOR signaling pathway in cancer: a rationale for cancer treatment. Biochem Pharmacol 2025; 232: 116729. https://doi.org/10.1016/j.bcp.2024.116729

[46] TENG JF, QIN DL, MEI QB, QIU WQ, PAN R et al. Polyphyllin VI, a saponin from trillium tschonoskii maxim. induces apoptotic and autophagic cell death via the ROS triggered mTOR signaling pathway in non-small cell lung cancer. Pharmacol Res 2019; 147: 104396. https://doi.org/10.1016/j.phrs.2019.104396

[47] ASNAGHI L, BRUNO P, PRIULLA M, NICOLIN A. mTOR: a protein kinase switching between life and death. Pharmacol Res 2004; 50: 545-549. https://doi.org/10.1016/j.phrs.2004.03.007

[48] EASLEY CA, BEN-YEHUDAH A, REDINGER CJ, OLIVER SL, VARUM ST et al. mTOR-mediated activation of p70 S6K induces differentiation of pluripotent human embryonic stem cells. Cell Reprogramming 2010; 12: 263-273. https://doi.org/10.1089/cell.2010.0011

[49] QIU ZX, SUN RF, MO XM, LI WM. The p70S6K Specific Inhibitor PF-4708671 Impedes Non-Small Cell Lung Cancer Growth. PLoS ONE 2016; 11: e0147185. https://doi.org/10.1371/journal.pone.0147185

[50] SHIN JM, JEONG YJ, CHO HJ, PARK KK, CHUNG IK et al. Melittin suppresses HIF-1α/VEGF expression through inhibition of ERK and mTOR/p70S6K pathway in human cervical carcinoma cells. PLOS One 2013; 8: e69380-NaN. https://doi.org/10.1371/journal.pone.0069380

[51] ZHANG YJ, DAI Q, SUN DF, XIONG H, TIAN XQ et al. mTOR signaling pathway is a target for the treatment of colorectal cancer. Ann Surg Oncol 2009; 16: 2617-2628. https://doi.org/10.1245/s10434-009-0555-9

[52] NEUFELD TP. TOR-dependent control of autophagy: biting the hand that feeds. Curr Opin Cell Biol 2010; 22: 157-168. https://doi.org/10.1016/j.ceb.2009.11.005

[53] GANLEY IG, LAM DH, WANG J, DING X, CHEN S et al. ULK1·ATG13·FIP200 Complex Mediates mTOR Signaling and Is Essential for Autophagy. J Biol Chem 2009; 284: 12297-12305. https://doi.org/10.1074/jbc.M900573200

[54] ZHU L, SHEN XB, YUAN PC, SHAO TL, WANG GD et al. Arctigenin inhibits proliferation of ER-positive breast cancer cells through cell cycle arrest mediated by GSK3-dependent cyclin D1 degradation. Life Sci 2020; 256: 117983. https://doi.org/10.1016/j.lfs.2020.117983

[55] WANG F, LI Z, CHEN L, YANG T, LIANG B et al. Inhibition of ASCT2 induces hepatic stellate cell senescence with modified proinflammatory secretome through an IL-1α/NF-κB feedback pathway to inhibit liver fibrosis. Acta Pharm Sin B 2022; 12: 3618-3638. https://doi.org/10.1016/j.apsb.2022.03.014

[56] CHEN Y, LIU J, ZHONG S, ZHANG T, YUAN J et al. Monotropein inhibits epithelial-mesenchymal transition in chronic colitis via the mTOR/P70S6K pathway. Front Pharmacol 2025; 16: 1536091. https://doi.org/10.3389/fphar.2025.1536091

[57] HAN W, YU F, CAO J, DONG B, GUAN W et al. Valproic Acid Enhanced Apoptosis by Promoting Autophagy Via Akt/mTOR Signaling in Glioma. Cell Transplant 2020; 29: 963689720981878. https://doi.org/10.1177/0963689720981878

Figure Legends

Figure 1. The suppressive effects of V9302 on the proliferation and growth in PC-9 and A549 cells. A) The chemical structure of V9302. B) The inhibitory rates of PC-9 and A549 cells at different concentrations of V9302 were evaluated at 24 h. C) Gln levels in PC-9 and A549 cells after V9302 treatment were measured using Gln assay kit. D) GSH levels were quantified with GSH assay kit. E,

F) Western blotting analysis for the protein expression of ASCT2 with GAPDH as loading control. The relative protein level was quantitated by Image J analysis software. G) The proliferation of the cells was assessed using EdU assay. H) Colony formation assay was carried out to analyze the cell proliferation. (I) Cell cycle distribution of PC-9 and A549 cells was measured with PI staining after V9302 treatment for 24 h (n=3, *$p < 0.05$ vs. 0 μM group).

Figure 2. V9302 administration induced apoptosis in PC-9 and A549 cells. A) Annexin V-FITC/PI staining was utilized to evaluate apoptosis in PC-9 and A549 cells after V9302 treatment for 24 h. B) JC-1 fluorescence staining was used to observe the changes of MMP in the cells. C) Western blotting analysis for the protein expression of Bax, Bcl-2, cleaved Caspase-3, cleaved Caspase-9, and cleaved PARP, with β-Tubulin as loading control. The relative protein level was quantitated by Image J analysis software (n=3, *$p < 0.05$ vs. 0 μM group).

Figure 3. V9302 restrained migration in PC-9 and A549 cells. A, B) Wound-healing assay for PC-9 and A549 cells after exposure to V9302. Migration images were captured at 0 h and 24 h after scratching. C, D) Transwell assay for migration in PC-9 and A549 cells after V9302 treatment for 24 h. E) Western blotting analysis for protein expression of E-cadherin, N-cadherin and vimentin, with GAPDH as loading control. The relative protein level was quantitated by Image J analysis software (n=3, *$p < 0.05$ vs. 0 μM group).

Figure 4. V9302 significantly increased intracellular ROS levels in PC-9 and A549 cells, and ROS accumulation played a pivotal role in mediating the antitumor effects. A) ROS levels in cells treated with varying concentrations of V9302 were assessed by flow cytometry. B) The protein expression of mTOR/p70S6K signaling pathway-related molecules in PC-9 and A549 cells was determined by Western blotting, with GAPDH as the internal control. C) Following NAC (2 mM) pretreatment, ROS levels were evaluated by flow cytometry. D) After NAC (2 mM) pretreatment, the protein expression of mTOR/p70S6K signaling pathway-related molecules was examined by Western blotting (n=3, *$p < 0.05$ vs. 0 μM group, $^{\#}p < 0.05$ vs. Control group).

Figure 5. mTOR activation attenuated the effects of V9302 on proliferation and apoptosis in PC-9

and A549 cells. A) CCK8 was applied to determine the viability of cells pretreated with MHY1485. B, C) Proliferation was assessed by EdU assay in cells pretreated with MHY1485 (2 μM). D) Apoptosis rates were measured via flow cytometry following MHY1485 (2 μM) pretreatment. E) The expression levels of Bcl-2, Bax, Caspase-3, Caspase-9, and PARP were evaluated by Western blotting after MHY1485 (2 μM) pretreatment, with β-Tubulin as the internal reference (n=3, *p < 0.05, **p < 0.01 vs. Control group).

Figure 6. mTOR activation attenuated V9302-mediated inhibition of migration in PC-9 and A549 cells. A) Transwell migration assay was performed to evaluate the migratory capacity of cells following MHY1485 (2 μM) pretreatment. B) Protein expression levels of E-cadherin, N-cadherin, and vimentin were analyzed by Western blotting in MHY1485-pretreated (2 μM) cells, with GAPDH as the internal reference (n=3, *p < 0.05, **p < 0.01 vs. Control group).

Figure 7. V9302 demonstrated *in vivo* anti-neoplastic effects. A) Macroscopic view of the tumor after treatment for 2 weeks in the two groups. D) body weight, C) tumor volume, and B) The tumor weight of mice processed with V9302. E) ELISA was employed to determine changes in the indicators of renal function (BUN and CRE) and liver function (AST and ALT). F) HE staining graphs of the liver, kidney, heart, spleen, and lung; scale bar=50 μm. G, H) TUNEL assay was employed to analyze the apoptosis of tumor cells; scale bar=50 μm. I, J) Representative IHC graphs of Ki67, cleaved Caspase-3 and E-cadherin; scale bar=50 μm (n=6, *p < 0.05, **p < 0.01 vs. Control group).

Figure 8. Schematic diagram of the mechanism of V9302 inhibits NSCLC via ROS-mTOR/p70S6K pathway. V9302 downregulates ASCT2 expression to restrict glutamine uptake, leading to an accumulation of intracellular ROS and subsequent inhibition of the mTOR/p70S6K pathway. This cascade effectively suppresses NSCLC cell proliferation and migration, while simultaneously inducing apoptosis.

Fig. 1 [Download full resolution image]

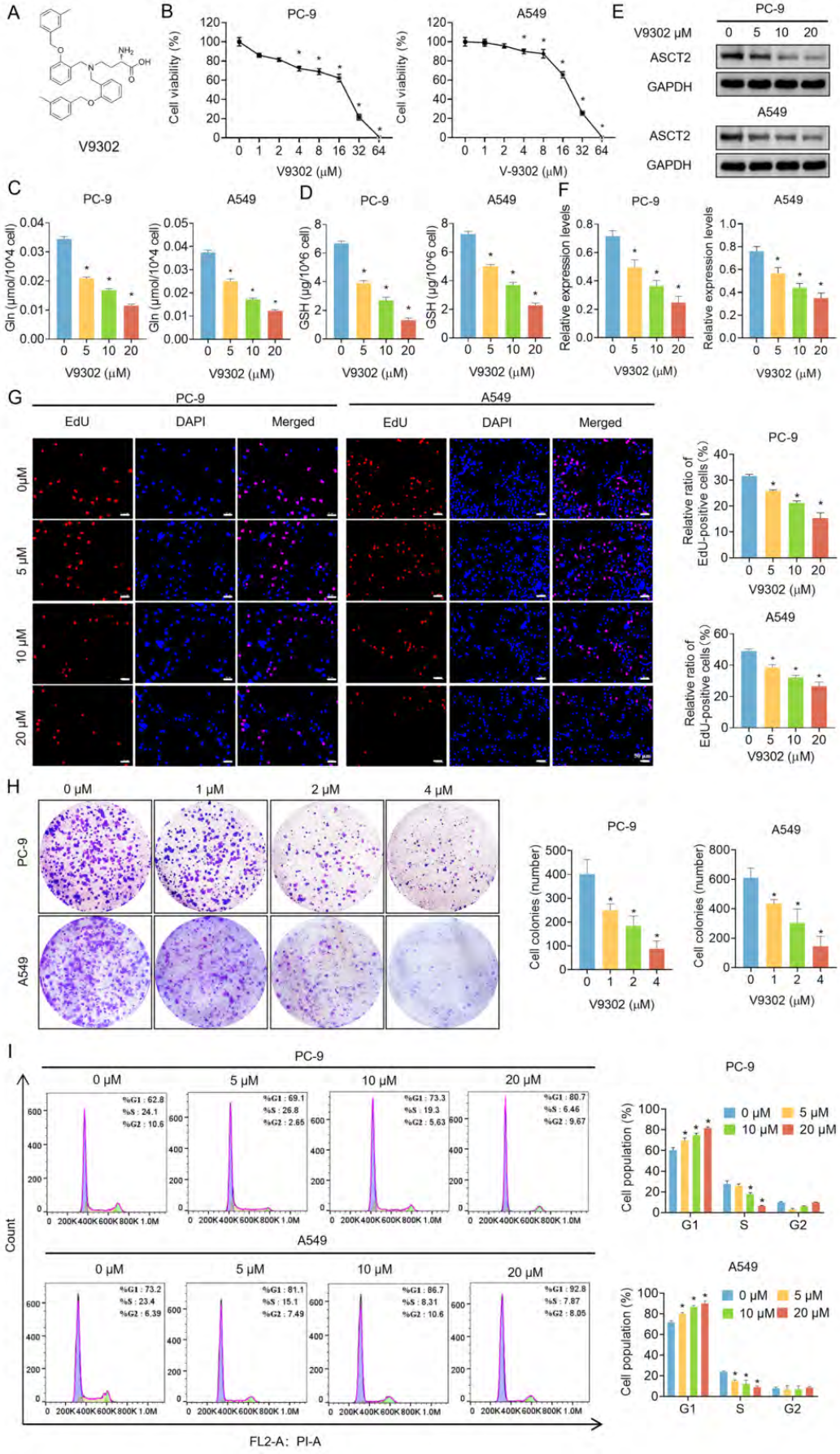

Fig. 2 [Download full resolution image]

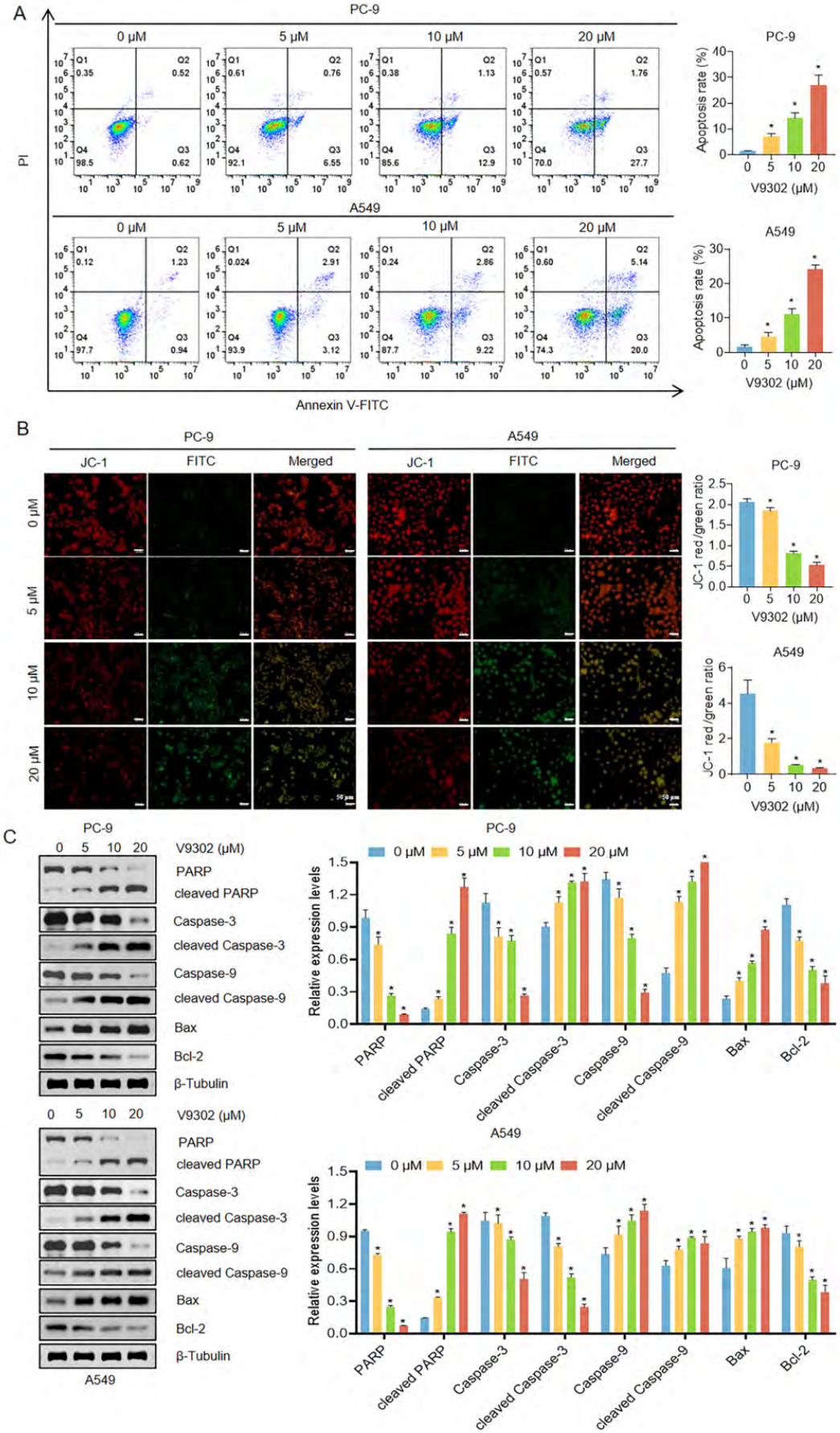

Fig. 3 [Download full resolution image]

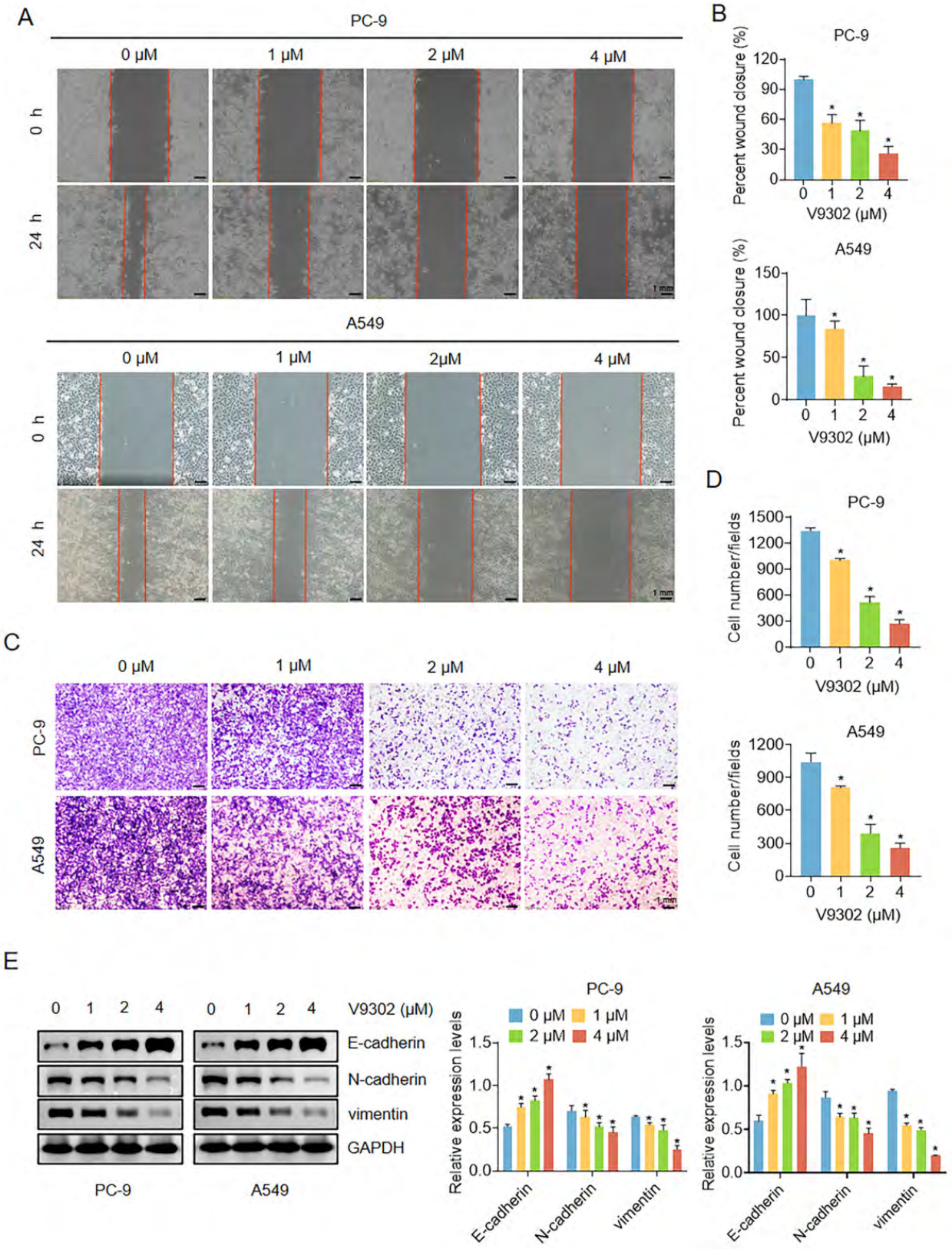

Fig. 4 Download full resolution image

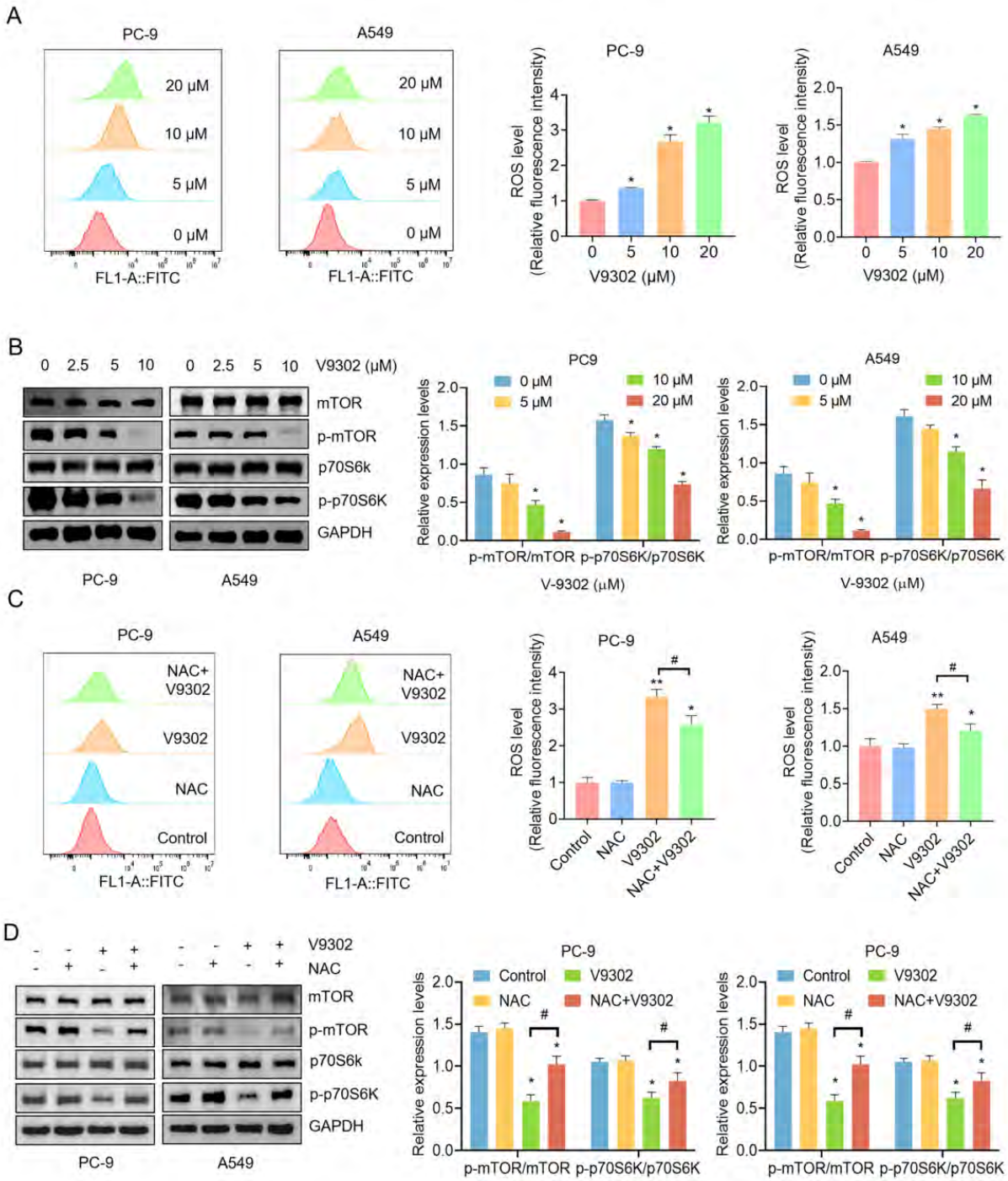

Fig. 5 Download full resolution image

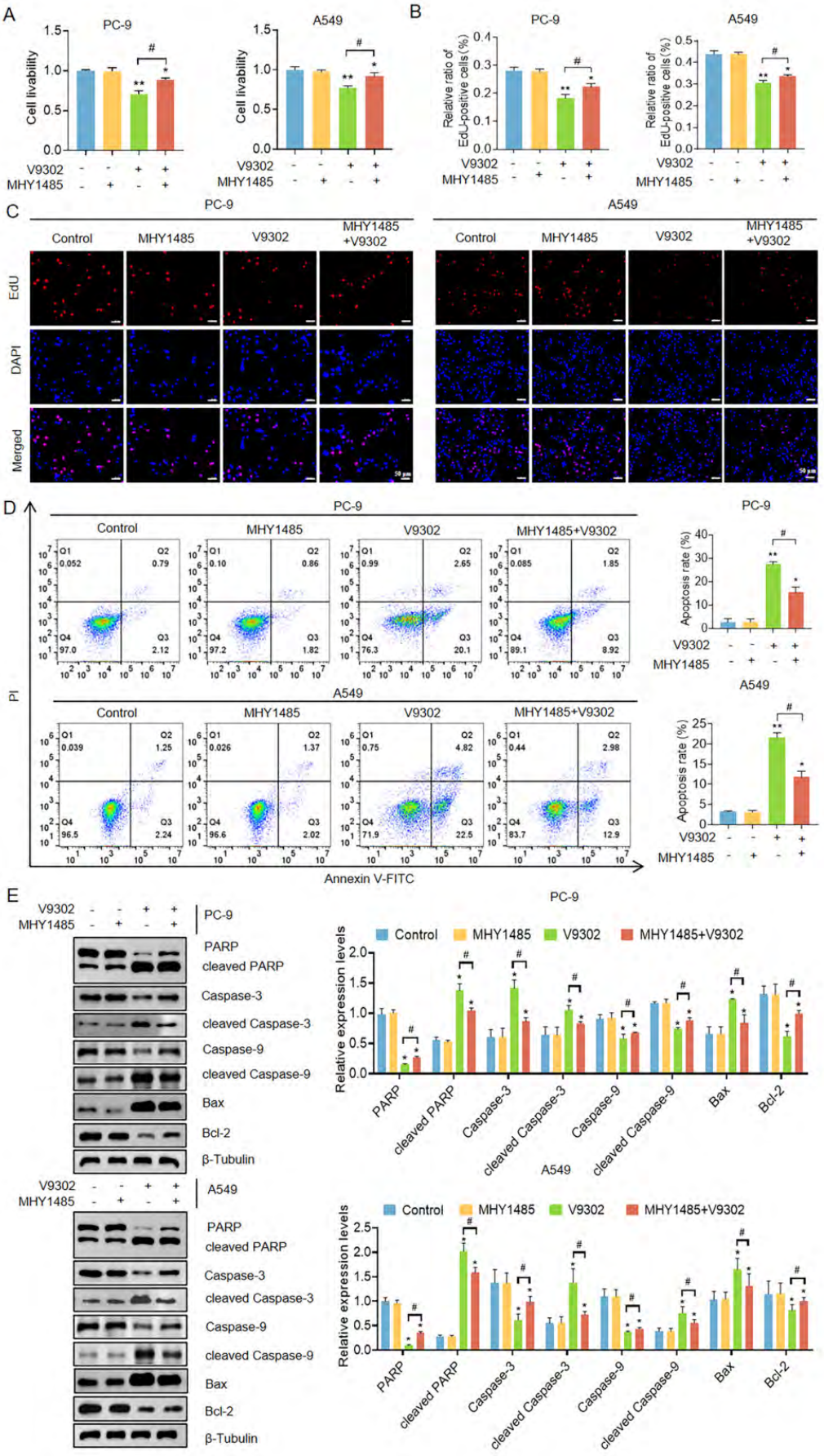

Fig. 6 Download full resolution image

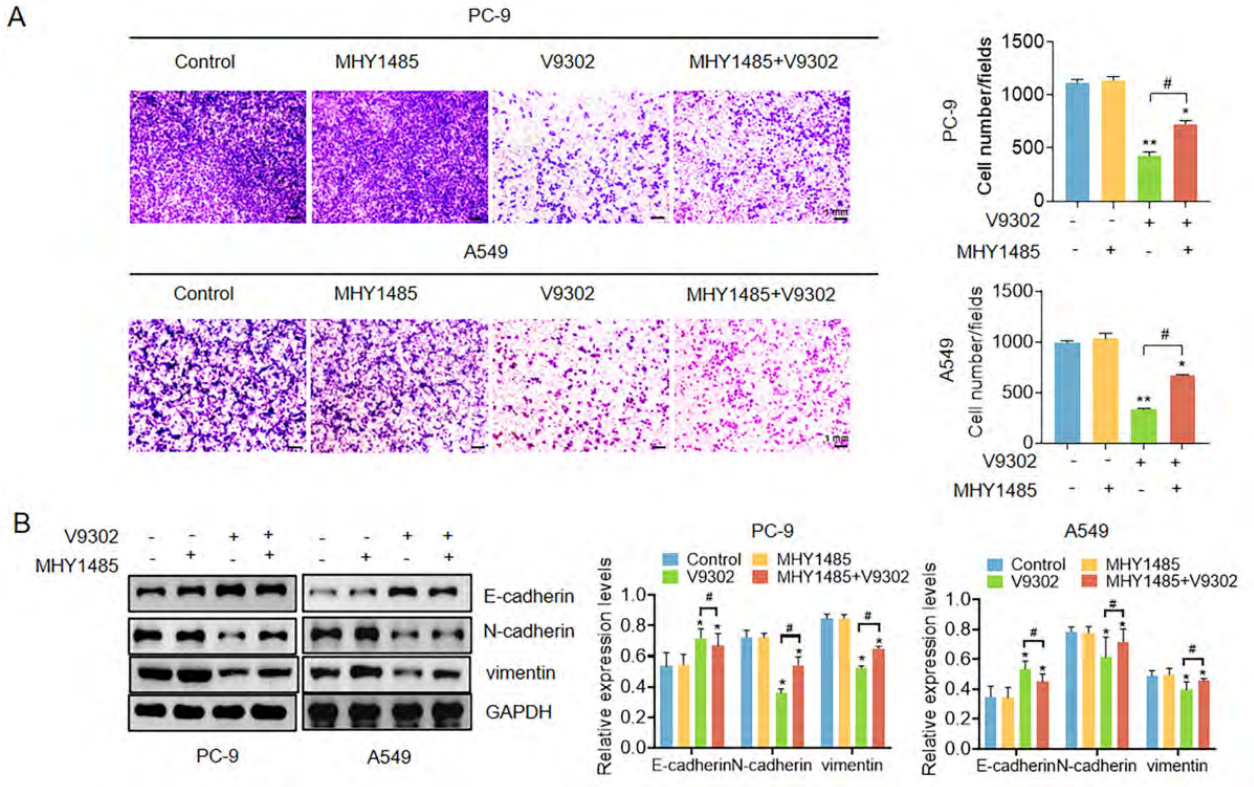

Fig. 7 [Download full resolution image]

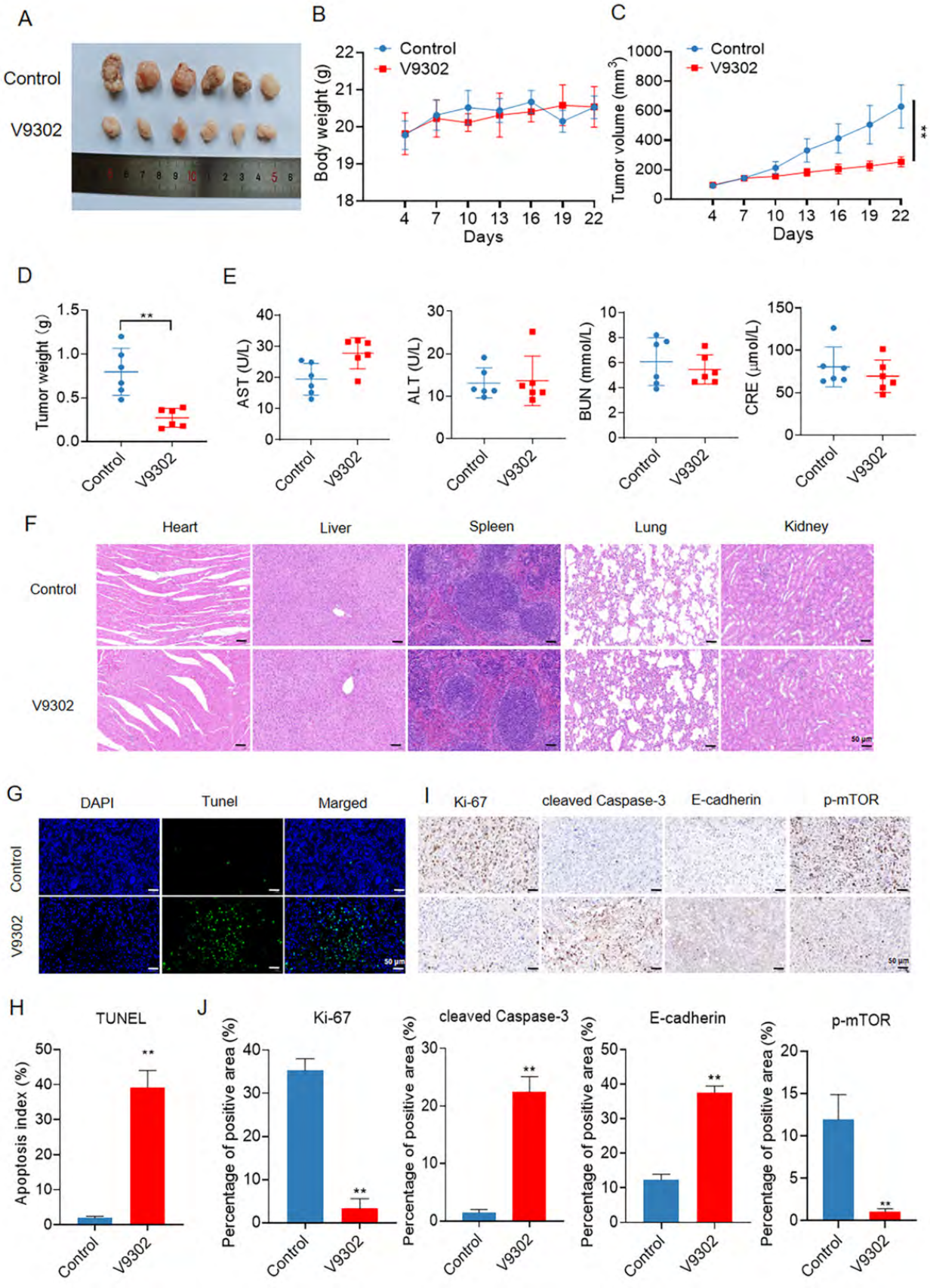

Fig. 8 Download full resolution image